Beam Shape Sensing Using Inverse Finite Element Method: Theory and Experimental Validation

M. GHERLONE, P. CERRACCHIO, M. MATTONE, M. DI SCIUVA and A. TESSLER

ABSTRACT

An inverse Finite Element Method (iFEM) is presented for beam and frame structures. The method is aimed at reconstructing the complete displacement field starting from in situ measurements of surface strains. A laboratory experiment is conducted on a simple cantilever beam subjected to various static loadings. Experimentally measured strains are used within a single-element iFEM model to assess the efficiency and predictive capability of the approach with respect to uncertainties and measurement errors that unavoidably affect real structures.

INTRODUCTION

Real-time *reconstruction* of the deformed shape of a structure is a key technology for Structural Health Monitoring (SHM) [1]. The computation of the displacement field is performed on the basis of in situ strain data computed in real time by a network of strain sensors. This inverse problem is commonly referred to as *shape sensing*.

Few approaches in the literature lead to practical algorithms applicable for real-time shape sensing of aerospace structures (for a more complete review refer to [1,2]). Ko [3] proposed a one-dimensional scheme based on classical beam theory, in which the deflection and cross-sectional twist angle of an aircraft wing are determined by establishing the position of the wing's neutral axis, using a representative finite element solution of a wing. The axial surface-strain measurements are specified at the nodes of a piecewise approximation of the idealized beam; the method is assessed using the strains from a FEM solution. Mainçon and co-workers, [4,5], developed a finite element formulation, seeking the solution for displacements and loads simultaneously. Starting from measured displacements and strains and requiring a priori knowledge of the material properties and a subset of applied loading, the formulation results in the number of unknowns that is three times the number of degrees-of-freedom (dof's) in the finite element discretization. In [5] the effect of modeling errors is investigated. The approach was also assessed on a damaged beam

Marco Gherlone, Priscilla Cerracchio, Massimiliano Mattone, Marco Di Sciuva: Politecnico di Torino, Department of Aeronautics and Space Engineering, Corso Duca degli Abruzzi 24, 10129 Torino, ITALY.
Alexander Tessler: NASA Langley Research Center, Structural Mechanics and Concepts Branch, Mail Stop 190, Hampton, VA 23681, U.S.A.

Report Documentation Page

Form Approved
OMB No. 0704-0188

1. REPORT DATE	2. REPORT TYPE	3. DATES COVERED
SEP 2011	**N/A**	**-**

4. TITLE AND SUBTITLE	5a. CONTRACT NUMBER
Beam Shape Sensing Using Inverse Finite Element Method: Theory and Experimental Validation	5b. GRANT NUMBER
	5c. PROGRAM ELEMENT NUMBER
6. AUTHOR(S)	5d. PROJECT NUMBER
	5e. TASK NUMBER
	5f. WORK UNIT NUMBER
7. PERFORMING ORGANIZATION NAME(S) AND ADDRESS(ES) **Department of Aeronautics and Space Engineering, Corso Duca degli Abruzzi 24, 10129 Torino, ITALY.**	8. PERFORMING ORGANIZATION REPORT NUMBER
9. SPONSORING/MONITORING AGENCY NAME(S) AND ADDRESS(ES)	10. SPONSOR/MONITOR'S ACRONYM(S)
	11. SPONSOR/MONITOR'S REPORT NUMBER(S)

12. DISTRIBUTION/AVAILABILITY STATEMENT
Approved for public release, distribution unlimited

13. SUPPLEMENTARY NOTES
See also ADA580921. International Workshop on Structural Health Monitoring: From Condition-based Maintenance to Autonomous Structures. Held in Stanford, California on September 13-15, 2011 . U.S. Government or Federal Purpose Rights License.

14. ABSTRACT
An inverse Finite Element Method (iFEM) is presented for beam and frame structures. The method is aimed at reconstructing the complete displacement field starting from in situ measurements of surface strains. A laboratory experiment is conducted on a simple cantilever beam subjected to various static loadings. Experimentally measured strains are used within a single-element iFEM model to assess the efficiency and predictive capability of the approach with respect to uncertainties and measurement errors that unavoidably affect real structures.

15. SUBJECT TERMS

16. SECURITY CLASSIFICATION OF:			17. LIMITATION OF ABSTRACT	18. NUMBER OF PAGES	19a. NAME OF RESPONSIBLE PERSON
a. REPORT	b. ABSTRACT	c. THIS PAGE			
unclassified	**unclassified**	**unclassified**	**SAR**	**8**	

using experimentally measured data. Tessler and Spangler [1] developed an inverse Finite Element Method (iFEM) for shear-deformable plate and shell structures. The formulation is based on a least-squares variational principle that allows the full-field reconstruction of the three-dimensional displacement vector from measured surface strains. An experimental assessment of the method was presented in [6,7], where the deformed shape of a slender beam is reconstructed by an iFEM shell model using Fiber-Bragg Grating (FBG) strain measurements. Recently, Gherlone [8,9] presented an iFEM formulation for shear-deformable beam and frame structures. Beam and frame shape-sensing analyses were performed for static [10] and dynamic [2] loadings using strain data from high-fidelity FEM models.

The paper presents a brief review of the iFEM variational formulation that incorporates experimentally measured strains within a simple inverse beam-frame element. The element is based on Timoshenko beam theory which includes the axial, bending, torsional and transverse shear deformations. A laboratory experiment is then discussed in which a thin-walled cantilevered beam is tested using a set of static loadings. The experimentally measured strain-rosette data are then used within a single inverse-beam element to model the entire beam. The modeling accuracy of the iFEM-reconstructed deformed shape of the beam is assessed by comparing the predicted displacements with those measured experimentally by the displacement transducers distributed along the beam's span.

INVERSE BEAM-FRAME FINITE ELEMENT FORMULATION

Consider an isotropic, straight beam-frame structural member of Young's modulus E, shear modulus G, and Poisson ratio ν (Figure 1(a)). The structural member is referred to a Cartesian coordinate system (x, y, z), where x is positioned along the centroidal and shear axis, and y and z are the cross-section's principal inertial axes. The frame member has length L, cross-sectional area A, area moments of inertia with respect to the y- and z-axis, I_y and I_z, and polar moment of inertia $I_P = I_y + I_z$.

Consistent with the hypotheses of Timoshenko beam theory (each cross-section remains flat and rigid with respect to thickness-stretch deformations along the y- and z-axis) [11] and neglecting axial warping due to torsion, the displacement field is

$$\begin{aligned} u_x(x,y,z) &= u(x) + z\theta_y(x) - y\theta_z(x) \\ u_y(x,y,z) &= v(x) - z\theta_x(x); \quad u_z(x,y,z) = w(x) + y\theta_x(x) \end{aligned} \tag{1}$$

where u_x, u_y, and u_z are the displacements along the x-, y-, and z-axes respectively; u, v, and w are the corresponding average displacements; θ_x, θ_y, and θ_z are the rotations about the three coordinate axes. The *kinematic variables*, $\mathbf{u} \equiv \left[u, \quad v, \quad w, \quad \theta_x, \quad \theta_y, \quad \theta_z \right]^T$ and their positive orientations are shown in Figure 1(a). The displacement field (1) gives rise to the linear strains

$$\begin{aligned} \varepsilon_x(x,y,z) &= e_1(x) + z\,e_2(x) + y\,e_3(x) \\ \gamma_{xz}(x,y) &= e_4(x) + y\,e_6(x); \quad \gamma_{xy}(x,z) = e_5(x) - z\,e_6(x) \end{aligned} \tag{2}$$

where the *strain measures* $\mathbf{e}(\mathbf{u}) \equiv \left[e_1, \quad e_2, \quad e_3, \quad e_4, \quad e_5, \quad e_6 \right]^T$ are given as

$$e_1 \equiv u_{,x}; \quad e_2 \equiv \theta_{y,x}; \quad e_3 \equiv -\theta_{z,x}; \quad e_4 \equiv w_{,x} + \theta_y; \quad e_5 \equiv v_{,x} - \theta_z; \quad e_6 \equiv \theta_{x,x} \tag{3}$$

The iFEM formulation reconstructs the deformed structural shape by minimizing a weighted least-squares functional Φ containing the strain measures obtained by in-situ strain sensors, $\mathbf{e}^{\varepsilon}$, and $\mathbf{e}(\mathbf{u})$ defined by Eqs. (3), i.e.,

$$\Phi(\mathbf{u}) = \left\| \mathbf{e}(\mathbf{u}) - \mathbf{e}^{\varepsilon} \right\|^2 \tag{4}$$

The $\Phi(\mathbf{u})$ functional is then discretized by C^0-continuous finite elements with the displacements $\mathbf{u}^h$ defined by

$$\mathbf{u}(x) \simeq \mathbf{u}^h(x) = \mathbf{N}(x)\mathbf{u}^e \tag{5}$$

where $\mathbf{N}(x)$ denotes C^0-continuous shape functions and $\mathbf{u}^e$ the nodal dof's. Consequently, the total least-squares functional is a sum of the N individual element contributions, $\Phi^e(\mathbf{u}^h)$, i.e., $\Phi = \sum_{e=1}^{N} \Phi^e$. Accounting for the axial stretching, bending, twisting, and transverse shearing, the element functional is given by [2]

$$\Phi^e(\mathbf{u}^h) \equiv \sum_{k=1}^{6} \lambda_k \, \Phi_k^e \tag{6}$$

where $\boldsymbol{\lambda} \equiv \left[\lambda_1^0, \quad \lambda_2^0 A^e, \quad \lambda_3^0 A^e, \quad \lambda_4^0, \quad \lambda_5^0, \quad \lambda_6^0 A^e \right]$, with $\lambda_k^0 \quad (k = 1,...,6)$ denoting dimensionless weight coefficients, and A^e the element's cross-sectional area. The six components of the element functional are given as the Euclidean norms

$$\Phi_k^e \equiv \frac{L^e}{n} \sum_{i=1}^{n} \left[e_k(x_i) - e_k^{\varepsilon i} \right]^2 \quad (k = 1,...,6) \tag{7}$$

where L^e is the element length, n is the number of strain sensors within an element, and x_i $(0 \le x_i \le L^e)$ are the positions at which the strain sensors are located, with the superscript εi denoting the strain measures that are computed from the strain sensor values (experimental values) at the x_i locations. Invoking Eqs. (2) and (5), the analytic element-level strain measures are expressed in matrix form as

$$\mathbf{e}(\mathbf{u}) = \mathbf{B}(x)\mathbf{u}^e \tag{8}$$

where the matrix $\mathbf{B}(x)$ contains the derivatives of the shape functions $\mathbf{N}(x)$. Substituting Eq. (8) into Eq. (7) and minimizing the element functional with respect to $\mathbf{u}^e$ results in the element matrix equation $\mathbf{k}^e\mathbf{u}^e = \mathbf{k}^e$, where $\mathbf{k}^e$ depends only on the

measurement locations x_i, whereas the vector $\mathbf{f}^e$ depends on the experimentally measured strains [9]. Assembly of the element contributions for the total problem discretization, while taking into account transformations from the element (local) to the global coordinate system, and upon specifying the problem boundary conditions, results in a non singular system of matrix equations of the form $\mathbf{KU} = \mathbf{F}$. The solution of these equations for **U** is efficient: the **K** matrix is inverted only once, since it is independent of the measured strains and remains unchanged for a given distribution of strain sensors. The **F** vector, however, is dependent on the measured strain values; thus, at any strain measurement update during deformation, the matrix-vector multiplication provides the solution for the unknown nodal displacement dof's contained in **U**.

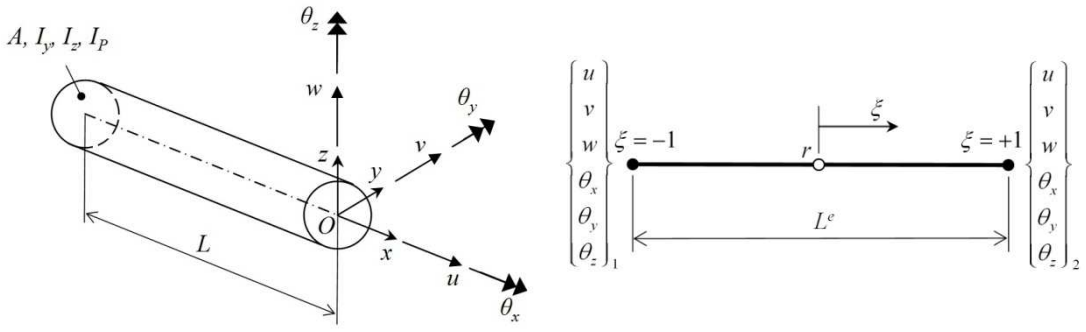

(a) (b)

Figure 1. (a) Beam geometry and kinematic variables, (b) inverse finite element geometry and dof's.

For frame structural elements loaded only by forces and moments at the end points, the strain measures can be shown to exhibit the following span-wise distributions: e_1, e_4, e_5, and e_6 are constant, whereas e_2 and e_3 are linear [9]. From Eq. (3), it is deduced that u and θ_x are linear, θ_y and θ_z parabolic, v and w cubic. Thus, the following interpolations are adopted [2,9,10] (also refer to Figure 1(b)):

$$
\begin{aligned}
u(\xi) &= \sum_{i=1,2} L_i^{(1)}(\xi) u_i; & \theta_x(\xi) &= \sum_{i=1,2} L_i^{(1)}(\xi) \theta_{xi} \\
v(\xi) &= \sum_{i=1,2} L_i^{(1)}(\xi) v_i - \sum_{j=1,r,2} N_j^{(3)}(\xi) \theta_{zj}; & \theta_y(\xi) &= \sum_{j=1,r,2} L_j^{(2)}(\xi) \theta_{yj} \\
w(\xi) &= \sum_{i=1,2} L_i^{(1)}(\xi) w_i + \sum_{j=1,r,2} N_j^{(3)}(\xi) \theta_{yj}; & \theta_z(\xi) &= \sum_{j=1,r,2} L_j^{(2)}(\xi) \theta_{zj}
\end{aligned}
\qquad (9)
$$

where $\xi \equiv (2x/L^e - 1) \in [-1,1]$ is a non-dimensional axial coordinate; the subscripts 1, r and 2 denote positions along the beam length at $\xi = -1$, $\xi = 0$, and $\xi = +1$, respectively; $L_i^{(1)}(\xi)$ $(i = 1,2)$ are linear Lagrange polynomials; $L_j^{(2)}(\xi)$ $(j = 1,r,2)$ are quadratic Lagrange polynomials. The cubic $N_j^{(3)}(\xi)$ $(j = 1,r,2)$ polynomials are obtained from standard cubic Lagrange polynomials by enforcing the transverse shear strain measures (e_4 and e_5) to be constant along the element (refer to [2] for the

expression of $N_j^{(3)}(\xi)$.) The element has fourteen dof's: six at each end node plus the rotations θ_{ym} and θ_{zm} at the mid-span. The two internal rotation dof's are condensed out statically to achieve a two-node, twelve dof element.

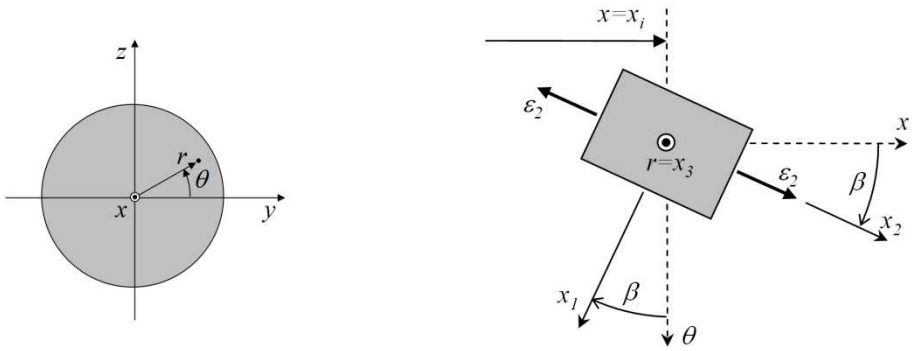

(a) (b)

Figure 2. (a) Orthogonal and cylindrical coordinate systems, (b) strain gauge location and coordinates.

A key step in the formulation is to compute the strain measures, $\mathbf{e}^{\boldsymbol{\varepsilon}}$, from the experimentally measured surface strains. We shall restrict the present analysis to the beam-frame members with circular cross-sections only, and employ the cylindrical coordinate system (θ, x, r) shown in Figure 2(a). A strain gauge is placed on the external surface ($r = R_{ext}$), at $x = x_i$, and is oriented along the θ and β angles (refer to Figure 2(b)). The relation between the measured strain ε_2 and the six strain measures at $x = x_i$ is [8,9]

$$\begin{aligned}\varepsilon_2(x_i,\theta,\beta) = e_1(x_i)\left(c_\beta^2 - \nu s_\beta^2\right) + e_2(x_i)\left(c_\beta^2 - \nu s_\beta^2\right)s_\theta R_{ext} + e_3(x_i)\left(c_\beta^2 - \nu s_\beta^2\right)c_\theta R_{ext} \\ + e_4(x_i)c_\beta s_\beta c_\theta - e_5(x_i)c_\beta s_\beta s_\theta + e_6(x_i)c_\beta s_\beta R_{ext}\end{aligned} \tag{10}$$

where $c_\theta \equiv \cos\theta$, $s_\theta \equiv \sin\theta$, $c_\beta \equiv \cos\beta$, and $s_\beta \equiv \sin\beta$. For the case of end-node forces and moments, the constant distributions of e_1, e_4, e_5, and e_6 and linear e_2 and e_3 can be determined requiring a total of eight strain measurements. This number may be reduced to six by invoking the equilibrium equations of Timoshenko beam theory which relate the bending moments (M_y, M_z) to the transverse shear forces (Q_y, Q_z)

$$\mathrm{dM}_z/\mathrm{d}x = \mathrm{Q}_y \Rightarrow EI_z e_{3,x} = k_y^2 GAe_5;\ \ \mathrm{dM}_y/\mathrm{d}x = \mathrm{Q}_z \Rightarrow EI_y e_{2,x} = k_z^2 GAe_4 \tag{11}$$

where k_y^2 and k_z^2 denote the shear correction factors [9,11].

EXPERIMENTAL RESULTS

The application of iFEM for beam and frame structures has been carried out using a laboratory experiment conducted at the *AERMEC* Laboratory of the Aeronautics and Space Engineering Department of Politecnico di Torino. The test article, shown in

Figure 3(a), is a thin-walled circular cross-section beam having thickness s=2 mm, external radius R_{ext}=40 mm and length L=800 mm. The material is a 6060 aluminum alloy (E=61,922 MPa, ν=0.33). The beam has been mounted on a test-bed in a cantilevered configuration with one end clamped between two couples of iron blocks locked together by twelve bolted connections. Four different load cases have been considered (Figure 3(b)): (i) tip vertical force, (ii) tip horizontal force, (iii) tip force inclined at 30° with respect to the horizontal y-axis of the cross-section, and (iv) tip vertical force applied at a distance b=300 mm from the center of the cross-section. The loading has been achieved by placing several weights on a cradle (for a total weight of F=26.83 Kg). For cases (i), (ii), and (iii), the cradle was linked to a screw at the center of the beam tip cross-section while; for load case (iv), the cradle was suspended to a proper lever arm provided by a thick plate embedded at the beam tip (Figure 3(a)).

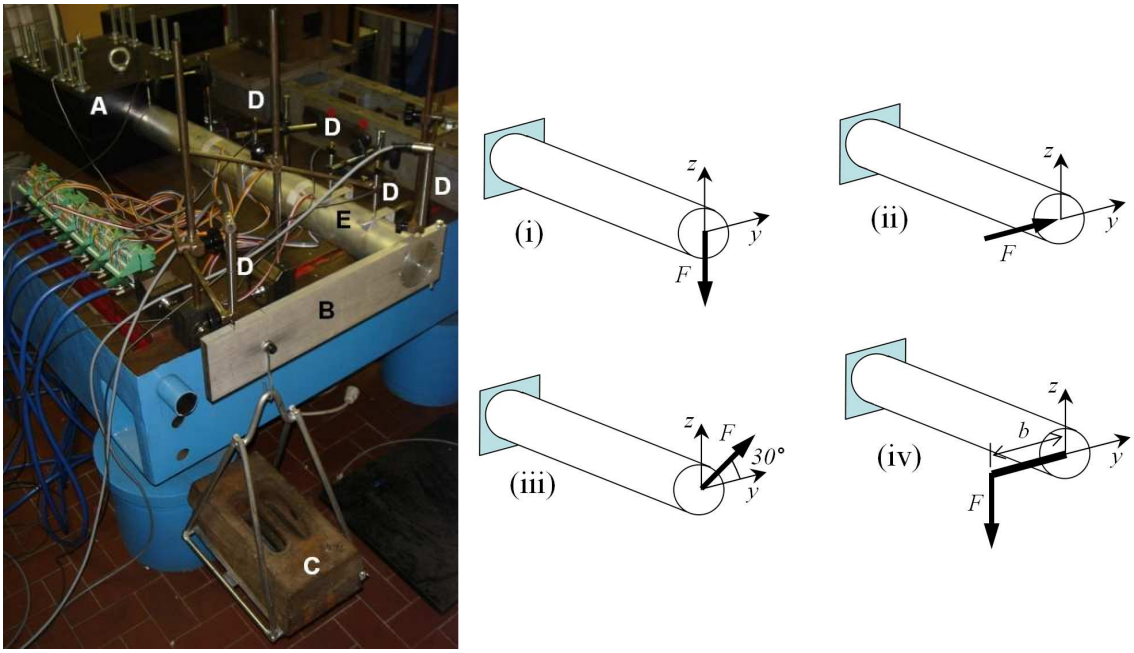

(a) (b)

Figure 3. (a) Experimental set-up (A: clamping system, B: lever arm for load case (iv), C: loading system, D: LVDT transducers, E: aluminum beam), (b) load cases.

Nine stacked strain rosettes have been placed at three different stations along the beam (x=L/3, L/2, 2L/3); for each station, the three rosettes are placed at θ=–120°, 0°, +120°, respectively. Each rosette has three strain gauge measuring at β=0°, 45°, 90° (Figure 2(b)). Table I shows the strain gauge configurations used. In the notation, the first number indicates the number of strain measurements, and the letter "E" signifies the use of Eqs. (11). LVDT measurements have also been taken at different locations along the beam length (Figure 3(a)) and used to assess the iFEM-recovered deflections and rotations. For all load cases, a single inverse element is used to model the entire beam, using $\lambda_k^0 = 1 \quad (k = 1,...,6)$, see Eq. (6).

Table II summarizes the experimental and iFEM results. For each loading, the measured deflections and rotations are shown, together with the percent difference with the corresponding iFEM predictions.

TABLE I. STRAIN GAUGE DISTRIBUTIONS
(ORIENTATIONS ARE EXPRESSED IN DEGREES).

Notation	Orientation (θ, β) at $x=L/3$	Orientation (θ, β) at $x=L/2$	Orientation (θ, β) at $x=2L/3$
6Ea	-	(-120,0), (-120,45), (0,0), (0,45), (120,0), (120,45)	-
6Eb	(-120,0), (0,0), (120,0)	-	(-120,0), (0,45), (120,0)
8a	(-120,0), (-120,45), (0,0), (120,45)	-	(0,0), (0,45), (120,0), (120,45)
8b	(-120,0)	(-120,0), (-120,45), (0,0), (0,45), (120,0), (120,45)	(120,0)

TABLE II. EXPERIMENTAL AND IFEM RESULTS: DEFLECTIONS AND ROTATIONS MEASURED BY LVDT AND PERCENT DIFFERENCE (IN BOLD) IN IFEM PREDICTIONS USING A SINGLE INVERSE-ELEMENT MODEL.

Load case (i)	Measured displacements (mm)		*w(L/2)*	*w(3L/4)*	*w(7L/8)*	*w(L)*		
			-0.648	-1.300	-1.635	-1.985		
	iFEM % difference	6Ea	**-9.48**	**-7.82**	**-5.11**	**-3.09**		
		6Eb	**-2.85**	**-2.45**	**-0.36**	**0.88**		
		8a	**-1.07**	**-0.86**	**0.01**	**2.22**		
		8b	**-1.52**	**-1.12**	**0.92**	**2.12**		
Load case (ii)	Measured displacements (mm)		*v(L/2)*	*v(3L/4)*	*v(7L/8)*	*v(L)*		
			0.636	1.272	1.648	1.994		
	iFEM % difference	6Ea	**-4.73**	**-3.70**	**-4.34**	**-2.61**		
		6Eb	**-4.00**	**-3.59**	**-4.58**	**-3.24**		
		8a	**-5.24**	**-3.98**	**-4.62**	**-2.95**		
		8b	**-2.87**	**-1.99**	**-2.87**	**-1.42**		
Load case (iii)	Measured displacements (mm)		*v(3L/4)*	*v(7L/8)*	*v(L)*	*w(3L/4)*	*w(7L/8)*	*w(L)*
			1.098	1.414	1.667	0.644	0.802	0.963
	iFEM % difference	6Ea	**-8.81**	**-8.44**	**-3.85**	**1.61**	**4.66**	**6.98**
		6Eb	**-4.83**	**-5.28**	**-1.48**	**-0.70**	**2.40**	**4.81**
		8a	**-5.97**	**-6.00**	**-1.79**	**-1.65**	**1.68**	**4.14**
		8b	**-4.35**	**-4.55**	**-0.46**	**1.93**	**4.83**	**6.75**
Load case (iv)	Measured displacements (mm) and rotations (rad)		*w(L/2)*	*w(3L/4)*	*w(7L/8)*	*w(L)*	$\theta_x(L)$	
			-0.664	-1.319	-1.647	-1.958	$3.5\text{x}10^{-3}$	
	iFEM % difference	6Ea	**-11.15**	**-8.70**	**-5.39**	**-1.37**	**-9.36**	
		6Eb	**-7.15**	**-5.69**	**-2.90**	**0.50**	**-5.23**	
		8a	**-4.10**	**-3.12**	**-0.58**	**2.51**	**-7.84**	
		8b	**-5.37**	**-3.83**	**-0.95**	**2.55**	**-9.36**	

In all loading cases and using any of the considered strain-gauge configurations, the iFEM-predicted tip deflections differ from the measured values by less than 7%. The deflections computed along the beam span exhibited slightly higher differences, however, not exceeding 12%. The iFEM model that used eight strain gauges generally produced more accurate predictions compared to the six-strain gauge configuration, with the exception of case (iv) corresponding to 6Eb which produced a slightly superior prediction for the tip twist rotation.

The results of this first experimental assessment of iFEM for beams confirm the accuracy and efficiency of the present formulation, particularly taking into account that only a single inverse element was used to model the beam.

CONCLUSIONS

An inverse finite element method (iFEM) has been presented for the full-field reconstruction of the Timoshenko-type beam-frame kinematics, using experimentally measured strains as input quantities in the formulation. The approach has been demonstrated on a cantilevered beam tested under several static loading cases in a mechanics laboratory. Strains measured by different sets of strain gauges, attached to the beam's external surface, have been employed in the inverse analyses. Using only a single-element model, the iFEM-reconstructed displacements and rotations compared favorably with those measured experimentally. The effectiveness of the iFEM modeling has been shown to depend on the layout and number of strain gauges. The results of the present effort also point towards the possibility of determining optimally distributed locations of the strain gauges in order to achieve further improvements in the shape-sensing predictions.

ACKNOWLEDGMENTS

The authors gratefully acknowledge the fundamental contribution to the experimental activity by Mr. Giuseppe Ruvinetti of Politecnico di Torino. The first author acknowledges the support of Politecnico di Torino within the *Young Researchers Program 2010*.

REFERENCES

1. Tessler, A., Spangler, J.L. 2005. A least-squares variational method for full-field reconstruction of elastic deformations in shear-deformable plates and shells, *Comput. Methods Appl. Mech. Engrg.*, 194:327–339.
2. Gherlone, M., Cerracchio, P., Mattone, M., Di Sciuva, M., Tessler, A. Dynamic shape reconstruction of three-dimensional frame structures using the inverse finite element method, III ECCOMAS Them. Conf. Comp. Meth. in Struct. Dynam. and Earthquake Engrg., Corfù, Greece.
3. Ko, W. L., Richards, W. L., Fleischer, V. T. 2009. Applications of the Ko displacement theory to the deformed shape predictions of the doubly-tapered Ikhana wing, *NASA/TP-2009-214652*:1–30.
4. Mainçon, P. 2004. Inverse FEM I: Load and response estimates from measurements, *II International Conference on Structural Engineering, Mechanics and Computation*, Cape Town, South Africa.
5. Barnardo, C., Mainçon, P. 2004. Inverse FEM IV: Influence of modelling error, *II International Conference on Structural Engineering, Mechanics and Computation*, Cape Town, South Africa.
6. Vazquez, S.L., Tessler, A. Quach, C.C., Cooper, E.G., Parks, J., Spangler, J.L. 2005. Structural health monitoring using high-density fiber optic strain sensor an in verse finite element methods, NASA Report, NASA/TM-2005-213761.
7. Quach C.C., Vazquez, S.L., Tessler, A., Moore, J.P., Cooper, E.G., Spangler, J.L. 2005. Structural anomaly detection using fiber optic sensors and inverse finite element method. AIAA Guid., Navig., and Cont. Conf. and Exhibit, San Francisco, California, AIAA-2005-6357.
8. Gherlone, M. 2008. Beam inverse finite element formulation, *LAQ Rep.* Politecnico di Torino, 1.
9. Cerracchio, P., Gherlone, M., Mattone, M., Di Sciuva, M., Tessler, A. 2010. Inverse finite element method for three-dimensional frame structures, *DIASP Rep.* Politecnico di Torino, 285.
10. Cerracchio, P., Gherlone, M., Mattone, M., Di Sciuva, M., Tessler A. 2010. Shape sensing of three-dimensional frame structures using the inverse finite element method, Vth European Workshop on Structural Health Monitoring, Sorrento, Italy.
11. Timoshenko, S. P. 1921. On the correction for shear of differential equations for transverse vibrations of prismatic bars, *Philosophical Magazine*, 41:744–746.